

Near-field spectra of quantum well excitons with non-Markovian phonon scattering

G. Mannarini*

National Nanotechnology Laboratory of CNR, via Arnesano 16, 73100 Lecce, Italy[†]

R. Zimmermann

Institut für Physik der Humboldt-Universität zu Berlin, Newtonstr. 15, 12489 Berlin, Germany

(Dated: July 4, 2018)

The excitonic absorption spectrum for a disordered quantum well in presence of exciton-acoustic phonon interaction is treated beyond the Markov approximation. Realistic disorder exciton states are taken from a microscopic simulation, and the deformation potential interaction is implemented. The exciton Green's function is solved with a self energy in second order Born approximation. The calculated spectra differ from a superposition of Lorentzian lineshapes by enhanced inter-peak absorption. This is a manifestation of pure dephasing which should be possible to measure in near-field experiments.

PACS numbers: 78.20.-e, 63.20.Ls, 73.43.Cd

I. INTRODUCTION

Unique information on semiconductor nanostructures even beyond the diffraction limit can be obtained using near-field spectroscopy. This opens the way to detect fine spectroscopic and structural details¹. Usual selection rules for optical transitions are broken, which allows one to observe also states which are dark in the far-field². The present record experiment is a spatial resolution of 30 nm which was achieved using a tapered optical fiber and an InAs self-assembled quantum dot (QD) sample³. Even with a less demanding setup using a resolution comparable to the wavelength of light, individual optical transitions can be seen due to their spatial and spectral position. Absorption spectra from quantum wells (QW) with interface fluctuations could be measured in transmission geometry through a metal aperture of 400 nm on a GaAs/AlGaAs sample whose substrate was removed⁴. This gives access to single exciton state absorption lineshapes, with the chance to detect deviations from a Lorentzian profile. Similar lineshapes are seen in photoluminescence (PL). Among others, Besombes *et al.*⁵ found that the PL from a single CdTe QD exhibits broad bands on the sides of the Lorentzian peak. This has been also seen in Fourier-transformed four wave mixing experiments by Borri *et al.*^{6,7}, who systematically studied the importance of the broad band with respect to the (Lorentzian broadened) zero phonon line (ZPL) as a function of confinement energy in InAs/InGaAs QDs.

However, using the standard Fermi's golden rule for the phonon scattering, only a Lorentzian broadened ZPL is expected for the absorption spectrum of a single exciton state. Phenomena which go beyond the framework of Fermi's golden rule (such as the phonon broad band) are often called quantum kinetic or non-Markovian (i.e. memory) effects. The broad band can be understood in terms of a non-perturbative coupling between electronic and phonon degrees of freedom. This goes back to the

Huang-Rhys theory of *F*-centers⁸, which considers intra-state (diagonal) coupling to phonons only. This problem can be solved exactly with the cumulant expansion (also known as Independent Boson Model⁹). Since off-diagonal level coupling is absent, the ZPL remains unbroadened. Within this model, different exciton-phonon couplings such as optical polar, acoustic piezoelectric, and deformation potential have been studied¹⁰. This model was recently extended to include off-diagonal coupling, successfully explaining why the ZPL get broadened even if real phonon-assisted transitions to other levels are not possible (pure dephasing)^{11,12}. Apart from the cumulant expansion, approaches based on various dynamical approximations have been used, too. For instance, a 4th order selfconsistent summation of diagrams allowed one to compare QW linewidths extracted from photon echo measurements^{13,14}. It was found that at elevated temperatures the linewidth broadening is mainly due to pure dephasing. However, a simple quantum disk model for computing the exciton wave functions was used in this case. The correlation expansion for the carrier-phonon interaction which was used in Ref.15 to model the coupling to both optical and acoustical phonons, is exact up to the 2nd order. However, neither Coulomb or disorder effects were considered there.

A consistent theoretical treatment which describes non-Markovian effects for *realistic*, disordered excitonic resonances from semiconductor QWs is, to the best of our knowledge, still missing. In this paper we face this problem accounting for both diagonal and off-diagonal coupling to acoustic phonons via deformation potential interaction. The excitonic self energy is taken in second Born (2B) approximation and integrated numerically. This approach reproduces both the real scattering processes leading to the major ZPL broadening and the level-diagonal pure dephasing responsible for the broad band. The resulting (near-field) absorption spectrum exhibits apart from the Lorentzian-broadened individual lines a superposition of broad bands which results in an

enhanced inter-peak absorption. We suggest that this effect of non-Markovian dynamics can be demonstrated in near-field measurements.

The paper is organized as follows: The theory with a presentation of different approximations for the self energy in Sect. (II) is followed by numerical results in Sect. (III), and the conclusions are given in Sect. (IV). Finally, two appendixes contain more technical details.

II. THEORY

To model a realistic QW with disorder it is convenient to start with disorder eigenstates of the exciton. If the disorder strength is much smaller than both the level distance of electron and hole confinement states and the exciton binding energy, the total exciton wave function (in envelope function and effective mass approximation) can be factorized as¹⁶

$$\Psi_\alpha(\mathbf{r}_e, \mathbf{r}_h) = u_e(z_e) u_h(z_h) \phi_{1s}(\boldsymbol{\rho}_e - \boldsymbol{\rho}_h) \psi_\alpha(\mathbf{R}), \quad (1)$$

where confinement $u_a(z_a)$ in growth direction z , in-plane exciton relative motion $\phi_{1s}(\boldsymbol{\rho})$, and in-plane center-of-mass (COM) wavefunction $\psi_\alpha(\mathbf{R})$ appear. Since the first two functions are independent of disorder, they have to be computed just once for the disorder-free QW. Then, it suffices to solve a single particle equation for the COM exciton states in two dimensions,

$$\left[-\frac{\hbar^2}{2M} \Delta_{\mathbf{R}} + V(\mathbf{R}) \right] \psi_\alpha(\mathbf{R}) = \epsilon_\alpha \psi_\alpha(\mathbf{R}). \quad (2)$$

The potential $V(\mathbf{R})$ accounts for interface disorder and is spatially correlated on the scale of the exciton relative motion,

$$V(\mathbf{R}) = \int d\mathbf{R}' \sum_{a=e,h} \eta_a^2 \phi_{1s}^2[\eta_a(\mathbf{R} - \mathbf{R}')] \frac{dE_a}{dL_z} \Delta L_z(\mathbf{R}'), \quad (3)$$

with mass ratios $\eta_e = M/m_h$ and $\eta_h = M/m_e$. The well width fluctuations $\Delta L_z(\mathbf{R})$ transfer into potential fluctuations via the derivative of the ideal electron and hole confinement energy dE_a/dL_z ¹⁷. As zero of energy, we take the ideal 1s exciton transition energy of the lowest sublevel transition hh1-e1 in a GaAs/Al_{0.3}Ga_{0.7}As QW of given width L_z .

Recently, Grochol *et al.*¹⁸ have critically questioned the factorization Ansatz Eq.(1). Calculations with the full in-plane electron-hole wave function gave systematically lower eigenenergies, while the wave functions showed only minor modifications compared to the factorization, at least in the low-energy part of the spectrum. Since in the present paper, we are interested in the low-energy tail of the absorption spectrum with well localized states, the factorization can be safely used.

The interaction with acoustic phonons is treated here as the main source of scattering and dephasing. Optical

phonon scattering is not important here since, at temperatures below room temperature, optical phonon absorption by the exciton states is unlikely. Further, piezoelectric scattering is neglected since the exciton wave functions are typically large in momentum space, leading to small matrix elements for this kind of coupling^{19,20}. Thus, only deformation potential interaction with longitudinal acoustic phonons is relevant.

This model leads to the following Hamilton operator for excitons (creation operators B_α^\dagger) and acoustic phonons (creation operators $a_{\mathbf{q}}^\dagger$ with three-dimensional momentum \mathbf{q} with (bulk like) dispersion $w_{\mathbf{q}} = u_S |\mathbf{q}|$) :

$$\begin{aligned} \mathcal{H} = & \sum_\alpha \epsilon_\alpha B_\alpha^\dagger B_\alpha + \sum_{\mathbf{q}} \hbar w_{\mathbf{q}} a_{\mathbf{q}}^\dagger a_{\mathbf{q}} \\ & + \sum_{\alpha\beta\mathbf{q}} t_{\alpha\beta}^{\mathbf{q}} (a_{\mathbf{q}}^\dagger + a_{-\mathbf{q}}) B_\alpha^\dagger B_\beta. \end{aligned} \quad (4)$$

The deformation potential matrix elements $t_{\alpha\beta}^{\mathbf{q}}$ are discussed in App. (A). We have neglected the spin degree of freedom which splits each localized exciton state into a bright doublet via the exchange interaction. This splitting is driven by COM anisotropy and has typical values of a few tens of μeV ¹⁷. It can be disregarded in calculating absorption spectra with not too high resolution.

Within linear response theory, the optical properties of the system are given by the one-exciton Green's function (exciton propagator)

$$G_{\alpha\beta}(t - t') = -i \langle \mathcal{T} B_\alpha(t) B_\beta^\dagger(t') \rangle \quad (5)$$

with time ordered finite-temperature expectation value. In frequency space, the Green's function obeys the Dyson equation (in what follows $\hbar = 1$ is used, and the frequency ω is understood to carry a small negative imaginary part, $\omega - i0$)

$$\sum_\eta [(\omega - \epsilon_\alpha) \delta_{\alpha\eta} - \Sigma_{\alpha\eta}(\omega)] G_{\eta\beta}(\omega) = \delta_{\alpha\beta}, \quad (6)$$

introducing the exciton self energy matrix $\Sigma_{\alpha\eta}(\omega)$. The absorption spectrum is proportional to

$$\alpha(\omega) = \text{Im} \sum_{\alpha\beta} m_\alpha^* G_{\alpha\beta}(\omega) m_\beta. \quad (7)$$

The optical interband matrix elements m_α are defined in App. (A).

For the self energy, we take the lowest order diagram for the exciton-phonon interaction shown in Fig. 1. It is called 2nd order Born (2B) approximation since the interaction appears just twice:

$$\Sigma_{\alpha\eta}(\omega) = \sum_{\beta\mathbf{q}} t_{\alpha\beta}^{\mathbf{q}} t_{\beta\eta}^{-\mathbf{q}} \left[\frac{1 + n(w_{\mathbf{q}})}{\omega - \epsilon_\beta - w_{\mathbf{q}}} + \frac{n(w_{\mathbf{q}})}{\omega - \epsilon_\beta + w_{\mathbf{q}}} \right]. \quad (8)$$

The phonons are assumed to be in equilibrium at the lattice temperature T , $n(w_{\mathbf{q}}) = 1/(\exp(w_{\mathbf{q}}/k_B T) - 1)$. The

two terms in Eq. (8) are related to phonon emission and absorption. Note that the internal line in Fig. 1 is understood to represent the bare exciton propagator. Taking instead a dressed propagator with shifted quasiparticle energy would be an improvement. Our calculations have shown that this (acoustic) polaron shift for the localized exciton states is of the order of a few μeV only, and we have chosen to neglect it everywhere.

An alternative derivation would start with the equations of motion for the exciton propagator which couples to mixed exciton-phonon operator expectation values (phonon-assisted density matrix). The next equation in the hierarchy is then decoupled in a way that two phonon operators can be combined into the phonon occupation function. Eliminating the phonon assisted density matrix from the equations leads to a differential equation of the exciton propagator with a scattering being essentially a time integration over the past. This kind of memory in the scattering is fully equivalent to the frequency dependence of the self energy in the diagrammatic approach. Further, the non-diagonality of the self energy $\Sigma_{\alpha\eta}(\omega)$ leads to cross correlations among individual excitons.

In the Markov approximation these correlations are neglected, but more importantly the frequency dependence of the self energy is dropped completely. In the time frame, this means to extract the exciton propagator from the scattering integral at the latest time, thus skipping any memory effect. Consequently, the temporal dynamics of the propagator reduces to an exponential decay with a constant damping γ_{α}^M . In this paper we go beyond this level of approximation, aiming at a full non-Markovian description which includes the non-diagonality and the memory (frequency dependence) in the self energy. For the sake of comparison, we discuss in the following subsections the solution of Eq. (6) at various levels of sophistication.

The radiative contribution to the self energy (radiative damping) will be neglected since it is tiny in thin QWs which have strongly localized excitons¹⁷.

A. Full non-Markovian level

The self energy Eq. (8) can be written in a more compact form by extending the energy integration to positive and negative values,

$$\Sigma_{\alpha\eta}(\omega) = \sum_{\beta} \int dE n(E) \frac{J_{\alpha\eta}^{\beta}(E)}{\omega - \epsilon_{\beta} + E}, \quad (9)$$

which accounts for both phonon absorption and emission. The coupling function

$$J_{\alpha\eta}^{\beta}(E) \equiv \text{sgn}(E) \sum_{\mathbf{q}} t_{\alpha\beta}^{\mathbf{q}} t_{\beta\eta}^{-\mathbf{q}} \delta(|E| - \omega_{\mathbf{q}}). \quad (10)$$

can be viewed upon as a phonon density of states weighted by coupling matrix elements. Its spectral range

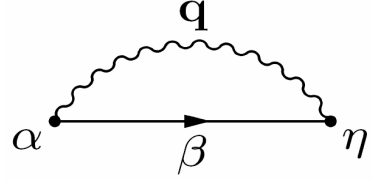


FIG. 1: Second order self energy diagram. The arrow denotes the exciton propagator, while the wiggly line stands for the phonon propagator. Each dot carries a coupling element t .

decides which exciton states are coupled to the phonon bath. It starts at least with a power of E^3 at small energies, as seen in App. (A). Since the exciton wave functions are real valued, the following symmetries hold: $J_{\alpha\eta}^{\beta}(E) = J_{\eta\alpha}^{\beta}(E)$ and $J_{\alpha\alpha}^{\beta}(E) = J_{\beta\beta}^{\alpha}(E)$. Thus, if we consider a system of N exciton states, $(N^3 + N)/2$ components of the coupling function have to be computed.

B. Markov approximation

The Markov approximation for the exciton-phonon dynamics is defined within our formalism by keeping only diagonal terms of the self energy and evaluating them at the exciton resonance (on-shell),

$$\Sigma_{\alpha\eta}(\omega) \rightarrow \delta_{\alpha\eta} \Sigma_{\alpha}^M, \quad \Sigma_{\alpha}^M \equiv \Sigma_{\alpha\alpha}(\omega = \epsilon_{\alpha} - i0). \quad (11)$$

Apart from the (small) polaron shift originating from the real part, this level of approximation implies a constant damping

$$\gamma_{\alpha}^M/2 = \text{Im} \Sigma_{\alpha}^M = \pi \sum_{\beta} n(\epsilon_{\beta} - \epsilon_{\alpha}) J_{\alpha\alpha}^{\beta}(\epsilon_{\beta} - \epsilon_{\alpha}). \quad (12)$$

(The factor 2 appears because γ_{α}^M is the decay rate of the intensity, which is proportional to the squared exciton propagator.) Thus, Eq. (6) reduces to a simple algebraic equation, and the absorption comes out as

$$\begin{aligned} \alpha(\omega) &= \sum_{\alpha} |m_{\alpha}|^2 \text{Im} \frac{1}{\omega - \epsilon_{\alpha} - i\gamma_{\alpha}^M/2} \\ &= \sum_{\alpha} |m_{\alpha}|^2 \frac{\gamma_{\alpha}^M/2}{(\omega - \epsilon_{\alpha})^2 + (\gamma_{\alpha}^M/2)^2}, \end{aligned} \quad (13)$$

which is a Lorentzian lineshape for each line. No broad bands are obtained within the Markov approximation. The rate γ_{α}^M is identical to the result of Fermi's golden rule. We notice that within the Markov approximation, only $(N^2 + N)/2$ components of the coupling function have to be computed.

C. Single state limit

As already mentioned, it is not possible to account for broad bands within the Markov approximation. In the single-state limit (uncoupled exciton states), the Markov rates Eq. (12) vanish since the coupling function $J_{\alpha\alpha}^\alpha(E)$ tends strongly to zero at zero argument $E = \epsilon_\alpha - \epsilon_\alpha$. Thus, in the absence of radiative damping, the absorption consists of delta lines. However, if we do not perform the Markov approximation, a composite absorption lineshape is obtained due to the frequency dependence of the self energy $\Sigma_{\alpha\alpha}(\omega)$. A broad band adds to the unbroadened zero phonon line. Its weight with respect to the total absorption area is $Z_\alpha = 1/(1 + S_\alpha)$, with the Huang-Rhys factor S_α stemming from the self energy derivative

$$S_\alpha = - \frac{d\text{Re}\Sigma_{\alpha\alpha}(\omega)}{d\omega} \Big|_{\omega=\epsilon_\alpha-i0} = \int dE n(E) \frac{J_{\alpha\alpha}^\alpha(E)}{E^2} > 0. \quad (14)$$

This result for Z_α agrees up to first order in S_α with the exact result from the independent Boson model, $Z_\alpha = \exp(-S_\alpha)$. However, the single-state solution neglects completely the inter-state scattering which leads to the Lorentzian broadening of the lines.

D. Semi-Markov approximation

In the full non-Markovian solution, both the Lorentzian broadening of the ZPL and the broad bands are obtained using the full self energy Eq. (9). However, the numerical cost of $O(N^3)$ coupling functions makes this treatment unfeasible for the large number N of excitons states covered by the focus of a typical near-field experiment. Thus, either one has to select fewer states, or one has to resort to another approximation which still preserves the main features of the absorption spectrum.

Aiming at this goal, we introduce the “Semi-Markov approximation” which neglects the off diagonal terms in the self energy and keeps the frequency dependence only in the fully state diagonal terms:

$$\begin{aligned} \Sigma_{\alpha\eta}(\omega) &\rightarrow \delta_{\alpha\eta} \Sigma_\alpha^{SM}(\omega), \\ \Sigma_\alpha^{SM}(\omega) &\equiv \int dE \frac{n(E) J_{\alpha\alpha}^\alpha(E)}{\omega - \epsilon_\alpha + E} \\ &+ \sum_{\beta \neq \alpha} \int dE \frac{n(E) J_{\alpha\alpha}^\beta(E)}{\epsilon_\alpha - i0 - \epsilon_\beta + E}. \end{aligned} \quad (15)$$

A linear expansion of $\Sigma_\alpha^{SM}(\omega)$ around the exciton pole ϵ_α shows (cf. App. B) that the ZPL has a reduced width

$$\gamma_\alpha^{SM} = \gamma_\alpha^M / (1 + S_\alpha). \quad (16)$$

The semi-Markov approximation is acceptable as long as the off diagonal elements of the self energy are small with respect to the differences between diagonal elements of

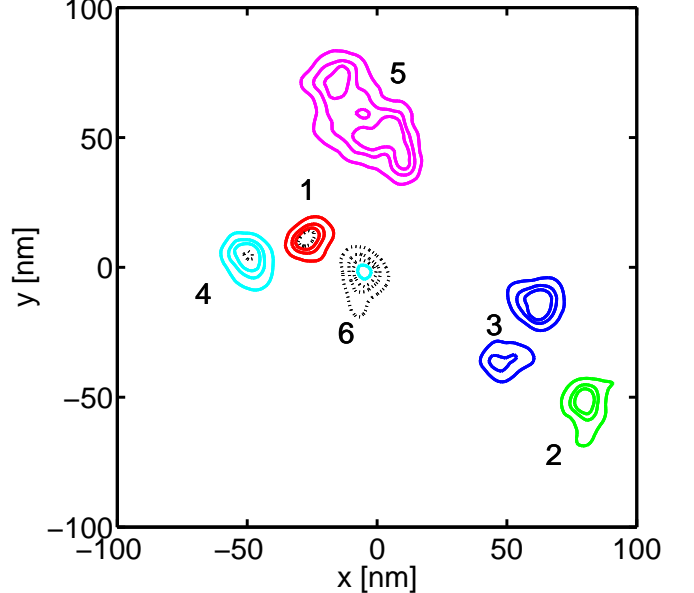


FIG. 2: (Color online) Probability amplitude of six exciton COM wave functions in a 5 nm wide GaAs/AlGaAs QW. The lines are drawn at 50, 30, and 10% of the peak probability of each wave function. Notice that state 1 and state 6 do overlap.

the matrix problem Eq. (6). Since these are dominated by the exciton eigenenergies, the semi-Markov approximation is expected to deviate markedly from the full non-Markov treatment only in spectral regions with a high density of overlapping states. Although much less demanding in computer power (only $(N^2 + N)/2$ coupling functions needed - as in the Markov approximation), both broad bands and broadening of the ZPLs are obtained in the semi-Markov approximation.

TABLE I: Material constants for bulk GaAs and other parameters used in the numerical simulations.

longitudinal sound velocity	u_S	5.33	nm/ps ^a
bulk mass density	ρ_M	5.37	g/cm ³ ^a
def. pot. electrons	D_c	-7000	meV ^a
def. pot. holes	D_v	+3500	meV ^a
exciton mass	M	0.300	m_0 ^b
in-plane electron mass	m_e	0.067	m_0
in-plane hole mass	m_h	0.233	m_0 ^b
QW width	L_z	5	nm
disorder strength	σ	4.75	meV
correlation length	a_B	9.9	nm
grid size	Δ_x	1.65	nm

^aAfter Ref.²¹

^bAfter Ref.²²

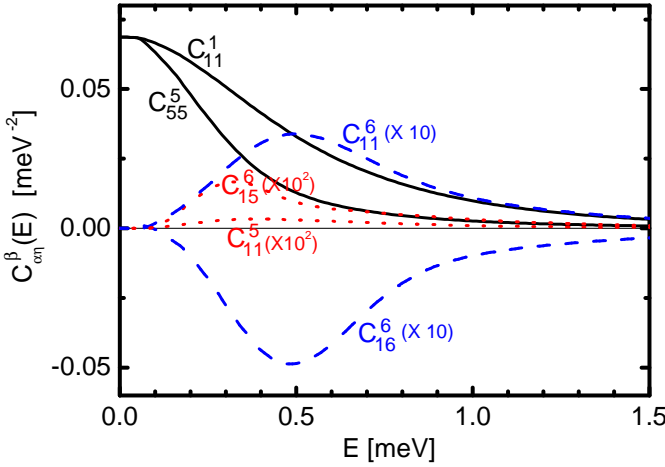


FIG. 3: (Color online) Selected components of the coupling function $C_{\alpha\eta}^{\beta}(E) \equiv J_{\alpha\eta}^{\beta}(E)/E^3$ for some of the states of Fig. 2. The off-diagonal components have been magnified by the factors given in brackets.

III. RESULTS

We present now numerical solutions of the theory developed in Sect. (II). The Schrödinger equation Eq. (2) has been discretized on a square grid with step size Δ_x . An uncorrelated potential corresponding to $(dE_a/dL_z)\Delta L_z(\mathbf{R})$ in Eq. (3) has been generated and convoluted with the relative exciton wave function, using parameters of a 5 nm wide GaAs/Al_{0.3}Ga_{0.7}As QW. The resulting disorder potential $V(\mathbf{R})$ is computed on the grid and has a correlation length close to the exciton Bohr radius a_B of this specific QW. The variance σ of this correlated potential has been adjusted to fit experimental results from the speckle analysis²³. The diagonalization of Eq. (2) on a simulation mesh of 128×128 grid points with periodic boundary conditions was achieved via an ARPACK-based package. All used material constants and simulation parameters are listed in Tab. I. In particular the in-plane hole mass is taken from an excitonic $k \cdot p$ calculation by Siarkos *et al.*²² which takes into account the heavy-light hole mixing. An effective hole mass of $m_h = 0.233 m_0$ could be extracted which describes satisfactorily the exciton COM motion for a wide range of quantum well thicknesses. We have used this hole mass for the effective-mass calculation in the present paper.

In Fig. 2 we display the amplitudes $|\psi_{\alpha}(\mathbf{R})|^2$ of six computed states, whose eigenenergies are contiguous. These states were selected by purpose of exhibiting various combinations of oscillator strength and spatial overlap to other states. In particular both quantities are large for $\psi_1(\mathbf{R})$ and both are small for $\psi_3(\mathbf{R})$. State $\psi_5(\mathbf{R})$ has large oscillator strength and small overlap, while for $\psi_6(\mathbf{R})$ the contrary holds. Here, we are restricted to six states only since we are going to compare the computationally most demanding spectra using the full self energy matrix Eq. (9) with other approximations.

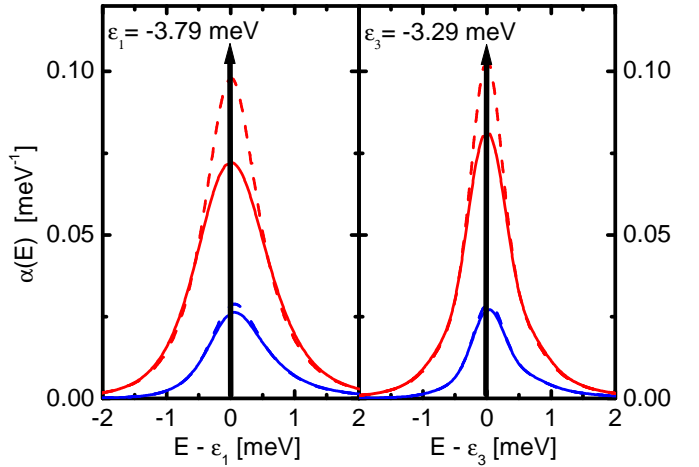


FIG. 4: (Color online) Absorption lineshape for a single state at $T = 40$ K (upper curves, red) and $T = 10$ K (lower curves, blue). Results from the 2nd Born approximation (solid lines) are compared with the exact solution (dashed) for state $\alpha = 1$ (left panel) and $\alpha = 3$ (right panel) of Fig. 2. The localization lengths are $\Lambda_1 = 16.4$ nm and $\Lambda_3 = 23.3$ nm. The arrows indicate the ZPLs, which correspond also to the Markov limit of the absorption spectra.

The coupling function $J_{\alpha\eta}^{\beta}(E)$ is formed using the eigenstates $\psi_{\alpha}(\mathbf{R})$ and represents the most time-consuming part of the numerical task. The fully diagonal components $J_{\alpha\alpha}^{\alpha}(E)$ are responsible for pure dephasing in the single-state limit. These components, divided by E^3 , are approximately Gaussians with FWHM inversely proportional to the localization length Λ_{α} of state α (full curves in Fig. 3 for $\alpha = 1$ and $\alpha = 5$). Their localization lengths (calculated from the inverse participation ratio) are 16.4 and 36.9 nm, respectively. Partially off-diagonal terms $J_{\alpha\alpha}^{\beta}(E)$ with $\beta \neq \alpha$ appear in the Markovian scattering rates γ_{α}^M (Eq. (12)) and are sensitive to the spatial overlap between $\psi_{\alpha}(\mathbf{R})$ and $\psi_{\beta}(\mathbf{R})$. In this sense, $\psi_1(\mathbf{R})$ overlaps with $\psi_6(\mathbf{R})$ about 100 times more effectively than with $\psi_5(\mathbf{R})$, according to Fig. 3. Finally, fully off-diagonal terms $J_{\alpha\eta}^{\beta}(E)$ with α, β, η all different account for deviations between the full solution with self energy Eq. (9) and the semi-Markov level with self energy Eq. (15). All nondiagonal terms of the coupling function vanish at $E \rightarrow 0$ with power E^4 due to the orthogonality of the exciton wave functions.

Having computed the coupling functions, the self energy at the desired level of approximation (single state, Markov, semi-Markov, or full non-Markov) can be easily generated. Using this input, the Green's function and the absorption spectrum are obtained. First we have checked the quality of our 2B treatment against the exact solution (Independent Boson Model) which is available in the single-state case only. In Fig. 4 we show the absorption spectra for state $\alpha = 1$ and $\alpha = 3$ of Fig. 2. The broad band stems from phonon absorption (left side of the ZPL) and phonon emission (right side). Therefore, the asymmetry evolves into a more symmetric shape as

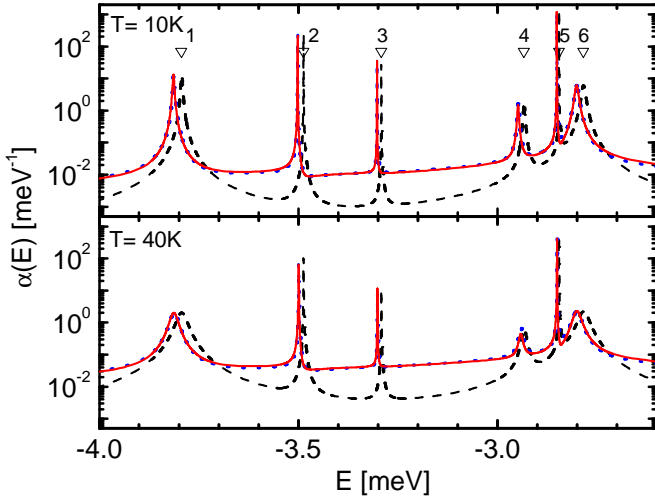


FIG. 5: (Color online) Absorption spectrum calculated in the Markov approximation (black dashes), with semi-Markov quality (blue dots), and with full non-Markovian quality (red full line) at lattice temperatures of $T = 10$ K (top panel) and $T = 40$ K (bottom panel). Notice the good agreement of semi-Markov and full non-Markovian results. No focus function is included. The triangles indicate the positions of the bare exciton eigenenergies.

temperature is raised. There is very good agreement between 2B and exact results at $T = 10$ K. However, at higher temperatures the broad band is underestimated in the self energy approach.

In Fig. 5 we display the absorption spectrum for the system of six exciton states. The Markovian spectrum (dashed) is simply a superposition of Lorentzian lines, whose widths are set by Fermi's golden rule, Eq. (12). Since the deformation potential matrix elements $t_{\alpha\beta}^q$ are sensitive to the spatial overlap of the COM wave functions (see App. (A)), states 2,3,5 exhibit narrower lines compared to states 1,4,6 which have a stronger overlap. The full non-Markovian spectrum is characterized by enhanced absorption between the single lines, as stressed by the logarithmic representation of Fig. 5. Furthermore a shift of the peak energies is observed (polaron shift). In the low energy part of the spectrum ($E \lesssim -3$ meV) the energetic spacing among the states is comparable to or larger than the width of diagonal elements of the coupling function (cf. Fig. 3). Thus, sidebands are clearly noticed although they overlap. They are about one order of magnitude larger than the superposition of the Lorentzian tails in the Markovian spectrum. Conversely, the energetic distance between states 5 and 6 is much smaller than the width of the corresponding coupling function $J_{\alpha\alpha}^q(E)$. In this region the inter-peak absorption is dominated by the Lorentzian tails of the ZPLs, and the individual broad bands cannot be easily resolved. A careful inspection reveals that the Lorentzian peak widths are smaller than in the Markovian case. According to Eq. (16) and Eq. (14), the width reduction scales with the Huang-Rhys factor and is more important for stronger lo-

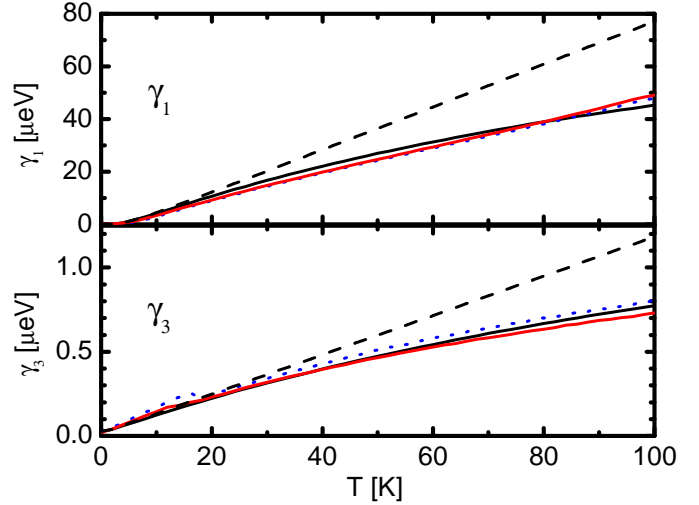


FIG. 6: (Color online) Temperature dependent ZPL widths γ_α for lines 1 and 3 of the full non-Markovian (solid red lines) and the semi-Markov spectrum (dotted blue lines) of Fig. 4. The simplified expression Eq. (16) (black solid lines) and the Markov rates γ_α^M (black dashed lines) are also displayed for comparison.

calized states and higher temperatures, as observed (cf. e.g. the peak of state 1). In Fig. 5 we also check the quality of the semi-Markov approximation against the full solution. The agreement is excellent at both $T = 10$ K and $T = 40$ K. Thus, pure dephasing is dominated by state-diagonal processes. A similar conclusion has been obtained in Ref. 14.

In Fig. 6 the temperature dependence of the linewidths of two selected states of Fig. 5 is studied. The reduced Markov width Eq. (16) fairly describes both full solution and semi-Markovian widths, as extracted from Lorentz fits in a narrow spectral window around the ZPLs. This linewidth reduction from Markov to non-Markov is a general feature and appears as soon as the spectral weight of the quasi particle is reduced. However, being a higher order effect in the coupling strength, one may ask how an inclusion of higher order terms would alter this finding. A consequent treatment of all diagrams up to 4th order in the cumulant expansion by Muljarov *et al.*¹² has shown that the reduction is indeed a pertinent feature. Its numerical value, however, might be quantitatively not correct when restricting to the level of 2nd Born approximation. In Fig. 6, a sublinear dependence of the linewidth on temperature is found for both states. This can be easily explained by noting that the Huang-Rhys factor increases nearly linear with T (cf. App. (B)).

Having tested the features of the semi-Markov approximation in Fig. 5 and Fig. 6, we apply it to a system of many exciton states. To come closer to the experimental situation of a near-field measurement, we have included a Gaussian focus of 50 nm width (FWHM of field intensity). Using the 50 lowest energy eigenstates of a disorder realization for a 5 nm wide QW we obtain the spectrum

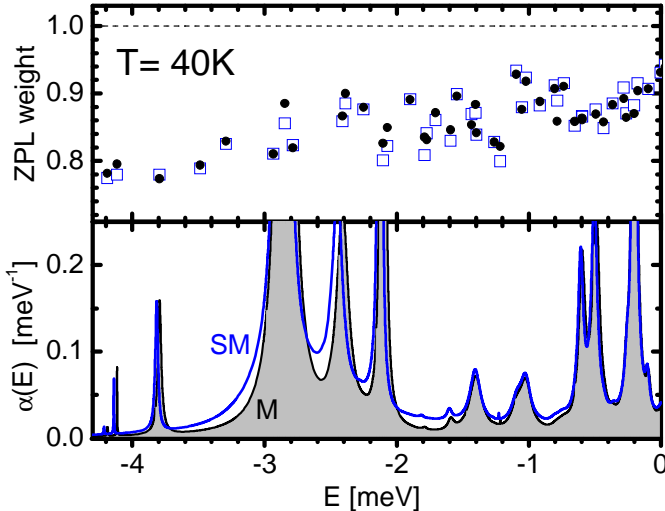


FIG. 7: (Color online) Top panel: ZPL weights $Z_\alpha = 1/(1 + S_\alpha)$ (blue squares) and $\Lambda_\alpha/(\Lambda_\alpha + bT)$ ratio (black circles) for a set of 50 exciton states at $T = 40$ K. A good agreement is predicted from Eq. (B5) and it is found using $b = 0.12$ nm/K. The dashed line is the constant ZPL weight within the Markov approximation. Bottom Panel: Markovian (shadowed area) and semi-Markovian (blue solid line) absorption spectrum for the same set of states at $T = 40$ K using a focus of 50 nm.

in Fig. 7 up to $E = 0$ meV which is the exciton energy in an ideal QW of the same width. In a near field geometry, the visibility of a state depends not only on its oscillator strength, but on the overlap with the illumination spot as well, as seen from Eq. (A2). Thus, several states in the range -3 meV $< E < -2$ meV appear especially strong in the present simulation. The absorption background between the peaks can be clearly seen on a linear scale in this spectral region. In the high energy tail ($E \approx 0$ meV) there is practically no difference between Markov and semi-Markov spectra. Even on a logarithmic scale both spectra are nearly identical (not shown). These observations can be explained considering the localization length Λ_α and the spectral separation of the exciton states. Λ_α is increasing across the spectrum from $\Lambda_2 = 17.2$ nm (the ground state is dark in the actual illumination geometry) up to $\Lambda_{50} = 54.1$ nm. Via the Huang-Rhys factor, this leads to an increasing ZPL weight (cf. App. (B)) which goes from $Z_2 = 0.77$ up to $Z_{50} = 0.92$, as seen in the top panel of Fig. 7. Thus, the importance of the non-Markovian broad bands (proportional to $1 - Z_\alpha$) decreases with photon energy. However, the observability of this effect strongly depends on the spectral separation of the resonances, as discussed for Fig. 5. The spectrally close doublet at about -4.2 meV e.g. does not show a distinct broad band, in spite of having a short localization length (large S_α). Thus, for observing non-Markovian effects in the absorption spectrum from QWs, it is necessary to position the near-field focus in such a way that states with small localization length and large spectral separation are excited.

A non-Markovian computation of the absorption which includes all optically active exciton states is at the moment beyond our computational possibilities. We expect somewhat broader ZPL peaks since more states would be available for phonon-mediated scattering. However, the broad band absorption between peaks is not expected to be modified as it is due to intra-state relaxation (first term on the rhs of Eq. (15)). Thus, a calculation of the absorption spectrum using all states will not reveal new features as compared to what we display in Fig. 7, at least within the semi-Markov approximation.

IV. CONCLUSIONS

In conclusion, we have developed a theoretical description of the exciton-acoustic phonon scattering in disordered QWs which goes beyond the Markov approximation. We have considered deformation potential coupling with acoustic phonons and realistic exciton states resulting from a microscopic simulation. A second order self energy approach is used for computing the absorption spectrum from the exciton propagator. At the Markov level the absorption is a superposition of Lorentzian peaks with widths defined by Fermi's golden rule, which results from phonon-assisted scattering between different states. At the full non-Markovian level, virtual scattering events on the same state are considered as well (pure dephasing). These processes manifest itself in broad absorption bands around Lorentzian peaks (ZPL) whose widths are smaller than according to Fermi's golden rule. We have also discussed a semi-Markov approximation in which a diagonal self energy is employed, but the important frequency dependence of the diagonal term is preserved. This allows to reduce the numerical task from $O(N^3)$ to $O(N^2)$, where N is the number of exciton states, while recovering all the important features of the complete solution. We have shown that the non-Markovian effect increases with a shorter localization length of the exciton wave function, and for low spectral density of states. A near-field setup could demonstrate these predictions experimentally.

Acknowledgments

Support from DFG in the frame of Sfb 296 is gratefully acknowledged. G. M. is thankful to Egor Muljarov (Berlin) for discussions and to Roberto Cingolani (Lecce) for support from CNR.

APPENDIX A: INTERACTION MATRIX ELEMENTS AND COUPLING FUNCTION

The matrix element for optical interband transitions between an exciton wave function $\Psi_\alpha(\mathbf{r}_e \mathbf{r}_h)$ and a light

field with momentum \mathbf{q} and field envelope $E(\mathbf{r})$ is given by

$$m_\alpha = \mu_{cv} \int d\mathbf{r} e^{-i\mathbf{q}\cdot\mathbf{r}} E(\mathbf{r}) \Psi_\alpha(\mathbf{r}, \mathbf{r}) \quad (\text{A1})$$

with the interband dipole moment μ_{cv} of the band edge states. The factorization Eq. (1) and transmission normal to the QW plane ($\mathbf{q}_\parallel = 0$) results in

$$m_\alpha = \mu_{cv} \phi_{1s}(0) O_{eh} \int d\mathbf{R} E(\mathbf{r}) \psi_\alpha(\mathbf{R}), \quad (\text{A2})$$

with $\phi_{1s}(0)$ as the relative exciton wave function at the origin, and O_{eh} the confinement overlap integral $O_{eh} = \int dz u_e(z) u_h(z)$.

Within the same factorization Ansatz, the deformation potential matrix element of Ref. 24 takes the form

$$\begin{aligned} t_{\alpha\beta}^{\mathbf{q}} = & \sqrt{\frac{\hbar w_{\mathbf{q}}}{2u_S^2 \rho_M V}} (\psi_\alpha \psi_\beta)_{\mathbf{q}_\parallel} \times \\ & \left[D_c K_e(q_z) \chi(\mathbf{q}_\parallel/\eta_e) - D_v K_h(q_z) \chi(\mathbf{q}_\parallel/\eta_h) \right] \end{aligned} \quad (\text{A3})$$

with deformation potential constants D_a , sound velocity u_S , mass density ρ_B , and normalization volume V . Further, we have defined Fourier transforms of the squared confinement and relative wave functions, and the COM overlap

$$\begin{aligned} K_a(q_z) &= \int dz u_a^2(z) e^{-iq_z z} \\ \chi(\mathbf{q}_\parallel) &= \int d\mathbf{p} \phi_{1s}^2(\rho) e^{-i\mathbf{q}_\parallel \cdot \rho} \\ (\psi_\alpha \psi_\beta)_{\mathbf{q}_\parallel} &= \int d\mathbf{R} \psi_\alpha(\mathbf{R}) e^{-i\mathbf{q}_\parallel \cdot \mathbf{R}} \psi_\beta(\mathbf{R}). \end{aligned} \quad (\text{A4})$$

In particular, for Gauss confinement states and a hydrogen-like relative motion we obtain:

$$\begin{aligned} K_a(q_z) &= \exp\left(-\frac{1}{2}(q_z L_a)^2\right) \\ \chi(\mathbf{q}_\parallel) &= (1 + (q_\parallel a_B/2)^2)^{-3/2}, \end{aligned} \quad (\text{A5})$$

where $L_e = 1.69$ nm and $L_h = 1.34$ nm. These two values result from a variational determination of the confinement levels in the 5 nm wide GaAs/AlGaAs QW. Other material constants for GaAs are listed in Tab. I.

Since the exciton states $\psi_\alpha(\mathbf{R})$ are numerically generated in Cartesian coordinates, we proceed with fast Fourier transformation along q_x , q_y , q_z and integrate accordingly Eq. (10) as

$$\begin{aligned} J_{\alpha\eta}^\beta(E) = & \frac{V}{(2\pi)^3} \int dq_x dq_y dq_z t_{\alpha\beta}^{\mathbf{q}} t_{\eta\beta}^{-\mathbf{q}} \times \\ & \delta(|E| - \hbar u_S \sqrt{q_x^2 + q_y^2 + q_z^2}) \end{aligned} \quad (\text{A6})$$

The delta function is used to integrate over q_z . Special care is taken to deal with the resulting square root singularities at the remaining integration limits. Each matrix element t contains a square-root of phonon energy, thus $J_{\alpha\eta}^\beta(E)$ starts at least with a power of E^3 .

APPENDIX B: ZPL WIDTH AND WEIGHT

In the semi-Markov approximation, the absorption is given by

$$\alpha(\omega) = \text{Im} \sum_\alpha \frac{|m_\alpha|^2}{\omega - \epsilon_\alpha - \Sigma_\alpha^{SM}(\omega)}. \quad (\text{B1})$$

For evaluating the ZPL width, we expand in Eq. (B1) the self energy around the pole ϵ_α . The real part at the resonance (polaron shift) $\text{Re}\Sigma_\alpha^{SM}(\epsilon_\alpha)$ is small and can be dropped, but its derivative has to be kept as

$$-\left. \frac{d}{d\omega} \text{Re}\Sigma_\alpha^{SM}(\omega) \right|_{\omega=\epsilon_\alpha-i0} = S_\alpha. \quad (\text{B2})$$

The imaginary part is taken as $\text{Im}\Sigma_\alpha^{SM}(\epsilon_\alpha - i0) = \gamma_\alpha^M/2$. Putting this into Eq. (B1) we end up with an absorption lineshape

$$\alpha(\omega \approx \epsilon_\alpha) = \sum_\alpha \frac{|m_\alpha|^2}{1 + S_\alpha} \text{Im} \frac{1}{\omega - \epsilon_\alpha - i\gamma_\alpha^{SM}/2}, \quad (\text{B3})$$

which has a reduced ZPL weight of $1/(1 + S_\alpha)$ and a reduced width $\gamma_\alpha^{SM} = \gamma_\alpha^M/(1 + S_\alpha)$.

At high temperatures, the phonon occupation can be replaced by $n(E) \rightarrow E/k_B T$. Together with the Gaussian shape of the diagonal coupling factor (see Fig. 3) we can evaluate the Huang-Rhys factor Eq. (14) in closed form

$$S_\alpha \approx \int dE \frac{k_B T}{E} E^3 A \exp\left[-\left(\frac{\Lambda_\alpha E}{u_s}\right)^2\right] \frac{1}{E^2} = b \frac{T}{\Lambda_\alpha}. \quad (\text{B4})$$

Thus, the ZPL weight is approximately given by

$$Z_\alpha = \frac{1}{1 + S_\alpha} \approx \frac{\Lambda_\alpha}{\Lambda_\alpha + bT}. \quad (\text{B5})$$

This approximation is getting better for less localized states, which can be seen in the top panel of Fig. 7.

^{*} Also at Institut für Physik der Humboldt-Universität zu Berlin, Newtonstr. 15, 12489 Berlin, Germany

[†] Electronic address: Gianandrea.Mannarini@unile.it

¹ E. Runge and C. Lienau, Phys. Rev. B **71**, 035347 (2005).

² U. Hohenester, G. Goldoni, and E. Molinari, Phys. Rev. Lett. **95**, 216802 (2005).

³ K. Matsuda, T. Saiki, S. Nomura, M. Mihara, and Y. Aoyagi, Appl. Phys. Lett. **81**, 2291 (2002).

⁴ J. R. Guest, T. H. Stievater, X. Li, J. Cheng, D. G. Steel, D. Gammon, D. S. Katzer, D. Park, C. Ell, A. Thranhardt, et al., Phys. Rev. B **65**, 241310(R) (2002).

⁵ L. Besombes, K. Kheng, L. Marsal, and H. Mariette, Phys. Rev. B **63**, 155307 (2001).

⁶ P. Borri, W. Langbein, U. Woggon, V. Stavarache, D. Reuter, and A. D. Wieck, Phys. Rev. B **71**, 115328 (2005).

⁷ P. Borri, W. Langbein, S. Schneider, U. Woggon, R. L. Sellin, D. Ouyang, and D. Bimberg, Phys. Rev. Lett. **87**, 157401 (2001).

⁸ C. B. Duke and G. D. Mahan, Phys. Rev. **139**, A1965 (1965).

⁹ G. D. Mahan, *Many-Particle Physics* (Plenum Press, 1990).

¹⁰ I. V. Bondarev, S. A. Maksimenko, G. Y. Slepyan, I. L. Krestnikov, and A. Hoffmann, Phys. Rev. B **68**, 073310 (2003).

¹¹ E. A. Muljarov and R. Zimmermann, Phys. Rev. Lett. **93**, 237401 (2004).

¹² E. A. Muljarov, T. Takagahara, and R. Zimmermann, Phys. Rev. Lett. **95**, 177405 (2005).

¹³ X. Fan, T. Takagahara, J. E. Cunningham, and H. Wang, Solid State Comm. **108**, 857 (1998).

¹⁴ T. Takagahara, Phys. Rev. B **60**, 2638 (1999).

¹⁵ B. Krummheuer, V. M. Axt, and T. Kuhn, Phys. Rev. B **65**, 195313 (2002).

¹⁶ R. Zimmermann, F. Grosse, and E. Runge, Pure and Applied Chemistry **69**, 1179 (1997).

¹⁷ R. Zimmermann, E. Runge, and V. Savona, *Theory of resonant secondary emission: Rayleigh scattering versus luminescence* in: *Quantum Coherence, Correlation and Decoherence in Semiconductor Nanostructures*, edited by T. Takagahara. Elsevier Science (2003).

¹⁸ M. Grochol, F. Grosse, and R. Zimmermann, Phys. Rev. B **71**, 125339 (2005).

¹⁹ E. Runge, *Excitons in semiconductor nanostructures*. in: *Solid State Physics*, edited by H. Ehrenreich and F. Spaepen. Academic Press, San Diego (2002).

²⁰ T. Takagahara, Phys. Rev. Lett. **71**, 3577 (1993).

²¹ K. Siantidis, V. M. Axt, and T. Kuhn, Phys. Rev. B **65**, 035303 (2001).

²² A. Siarkos, E. Runge, and R. Zimmermann, Phys. Rev. B **61**, 10854 (2000).

²³ G. Kocherscheidt, W. Langbein, G. Mannarini, and R. Zimmermann, Phys. Rev. B **66**, 161314(R) (2002).

²⁴ T. Takagahara, Phys. Rev. B **31**, 6552 (1985).